J. Fluid Mech. (2003), *vol.* 496, *pp.* 63–72.
DOI: 10.1017/S0022112003006530 Printed in the United Kingdom

Organized modes and the three-dimensional transition to turbulence in the incompressible flow around a NACA0012 wing

By Y. HOARAU[1], M. BRAZA[1], Y. VENTIKOS[2]†, D. FAGHANI[3] AND G. TZABIRAS[4]

[1]Institut de Mécanique des Fluides de Toulouse, CNRS/INPT UMR N°5502, Toulouse, France

[2]Laboratory of Thermodynamics in Emerging Technologies, ETHZ, Zurich, Switzerland

[3]Euro-American Institute of Technology, CERAM/EAI Tech, Sophia Antipolis, France

[4]National Technical University of Athens, P.O. Box 64070, Athens, Greece

(Received 15 January 2003 and in revised form 3 September 2003)

The transition to turbulence in the incompressible flow around a NACA0012 wing at high incidence is studied by DNS in the Reynolds number range 800–10 000. Two main routes are identified for the two-dimensional transition mechanisms: that to aperiodicity beyond the von Kármán mode via a period-doubling scenario and the development of a shear-layer instability, forced by the fundamental oscillation of the separation point downstream of the leading edge. The evolution of the global parameters as well as the variation law of the shear-layer instability wavelength are quantified. The history of the three-dimensional transition mechanisms from a nominally two-dimensional flow structure is identified beyond the first bifurcation, as well as the preferred spanwise wavelengths.

1. Introduction

The transition to turbulence in the flow around airfoils has, until recently, received less attention than similar configurations involving bluff-body wakes. Research on unsteady flows around airfoils has focused on the high-Reynolds number range and especially on pitching motion analysis related to the dynamic stall. This interest is justified by the importance of the pitching motion of lifting bodies in the avionics industry and especially rotorcrafts. However, there is a major interest, both from a fundamental and industrial point of view, on the inherent unsteady flow around airfoils and wings: the spontaneous appearance of unsteadiness with steady external conditions. There is particular interest in examining the natural transition to turbulence governing this kind of flow, because of the development of important organized modes that persist at the high Reynolds number range. From a practical point of view, the transition mechanisms lead to a substantial growth of the mean values and amplitudes of the global parameters, an issue that is important in both aerodynamics and in fluid–structure interaction.

There are few analyses in the literature on the two-dimensional unsteady separation at moderate Reynolds numbers. Mehta & Lavan (1975) in a pioneering work simulated the starting separation vortex in a flow at low Reynolds numbers. A

† Present address: Department of Engineering Science, University of Oxford, Parks Road, OX1 3PJ, UK.

comprehensive review of separation as well as of dynamic stall can be found in McCroskey (1982). The birth of natural transition in incompressible or subsonic flow regimes was studied by Pulliam & Vastano (1993) up to Reynolds number 3000, and by Ventikos, Tzabiras & Braza (1993), and in the transonic regime by Bouhadji & Braza (2002) up to Reynolds number 10 000.

Regarding the birth of the organized modes, there is little available knowledge of the three-dimensional mechanisms or the evolution of these modes over a wide, moderate Reynolds number range in the incompressible flow regime. The present paper focuses on the early stages of the natural transition, associated with the development of organized modes as the Reynolds number increases. The geometry chosen is the NACA0012 wing at a high angle of incidence (20°), ensuring a massively detached flow in a wide Reynolds number range. This study is based on time-dependent Navier–Stokes simulation, in two and three dimensions. The following points will be discussed:

(i) identifying the successive changes that the flow undergoes as the Reynolds number increases, as well as the related instability modes;

(ii) analysing in detail the shear-layer transition under the nonlinear interaction with the von Kármán mode in the higher Reynolds number range;

(iii) analysing the development of the three-dimensional transition from a nominally two-dimensional flow configuration subject to the von Kármán mode, which is strongly asymmetric due to the lifting body configuration.

2. Governing equations and numerical method

The governing equations are the continuity and the Navier–Stokes equations for an incompressible fluid. The numerical method is based on the pressure–velocity formulation employing a predictor–corrector pressure scheme and staggered grids for velocity and pressure. Two algorithms with similar features, both based on this methodology, have been used for the two-dimensional study, both leading to practically the same results. The first one is an implicit form of an originally explicit scheme by Amsden & Harlow (1970), extended in the present case to unsteady flows. The details can be found in Braza, Chassaing & Ha-Minh (1986). The other is a SIMPLE-type implicit algorithm, described in Tzabiras, Dimas & Loukakis (1986). The space derivatives are discretized by using central differences. The methodology in both cases is second-order accurate in space and time. The equations are written in orthogonal curvilinear systems.

For the three-dimensional cases, a three-step fractional time scheme (based on Douglas 1962 for the diffusion equations) has been extended to the convection–diffusion unsteady Navier–Stokes solution, as described by Persillon & Braza (1998). This scheme employs an alternating direction implicit method, leading to the solution of tridiagonal systems by a very fast algorithm. This is vital for realistic three-dimensional computations. The equations are written in general curvilinear coordinates. The numerical algorithm is fully parallelized for distributed memory architectures (Hoarau *et al.* 2001).

The boundary conditions are free stream at the inlet boundary and non-reflective absorption conditions for the outlet boundary, as specified by Jin & Braza (1993) to minimize very efficiently any feedback effect in the incompressible flow regime. The impermeability and adherence conditions are specified for the solid wall. C type grids are employed. Typical grids used for the two-dimensional simulations are 250×160, 450×200 to 1000×400 and the time step is $\Delta t = 0.001$. The grid used for the three-dimensional simulation is $(413 \times 70 \times 90)$. The spanwise length of the computational

domain is $4c$ and $12c$, both providing the same kind of three-dimensional phenomena; c represents the chord length and $Re = U_\infty c/\nu$ is the Reynolds number.

A very detailed and careful study of the choice of numerical parameters and dimensions of the computational domain, in respect of the grid and the spanwise distance independence of the results has been conducted, and for the two-dimensional study (Hoarau 2002; Ventikos 1995). The runs are carried out on the supercomputers SP3, SP4 and Origin 3000 of the national supercomputer centres CINES, IDRIS and CALMIP.

3. The first stages of the two-dimensional transition

First, computations are carried out in the very low Reynolds number regime (around $Re = 5$) showing a fully attached steady flow. As the Reynolds number increases, a small attached vortex is created near the trailing edge and grows with the Reynolds number. Near Reynolds number 70, where the bubble has attained a length nearly 40% the chord, unsteady separation starts and a very regular vortex shedding appears. The vortex shedding pattern is attained at $Re = 450$. At $Re = 800$, the vortex shedding motion is very regular. This regime is analysed in detail in the present study with respect to the two- and three-dimensional transition mechanisms. Beyond Reynolds number 800, the vortex shedding regularity is attenuated and other dominant frequencies appear, which are fractions of the fundamental, up to $Re = 2000$. As the Reynolds number increases further, the transition process becomes more complex, because of the development of a shear-layer instability as an incommensurate mode, analysed in § 3.2.

Two different mechanisms can be identified as the Reynolds number increases.

3.1. *The period-doubling mechanism*

The first mechanism corresponds to the evolution of the von Kármán instability and is closely related to a period-doubling, scenario, as is clearly shown in the spectra of the numerically obtained signals for increasing Reynolds number in the range (800–1600) (figure 1). The appearance of the first subharmonic of the main vortex shedding frequency can be physically justified by the fact that at a higher Reynolds number, the shed vortex close to the trailing edge is weakened at exactly $2T$ (T being the vortex shedding period) by the opposite vortex which starts being shed. This illustrates the phenomenon of period doubling, which is characterized by an energy–vorticity exchange process. This mechanism becomes dominant whenever the externally supplied energy (Reynolds number) to the system becomes higher than a critical value, in the context of the non-antisymmetric vortex shedding mode, owing to the lifting-body configuration. Recall that this kind of mechanism does not appear in the case of symmetric von Kármán vortex shedding, as for example in flows past bluff bodies.

The period-doubling mechanism appears repeatedly as the Reynolds number increases further, and it yields spectra with four, eight, ... peaks. The details of the period-doubling mechanism in the sense of Feigenbaum chaos (Feigenbaum 1978) have been studied by Pulliam & Vastano (1993) and Ventikos *et al.* (1993), among others. Our results compare very favourably with the ones obtained by Pulliam & Vastano, where such comparisons are possible. The time and space resolution employed in the present study is higher than in those two studies and this allows an accurate evaluation of the energy spectra and of the corresponding attractors corresponding to these successive changes. The attractor associated with each Reynolds

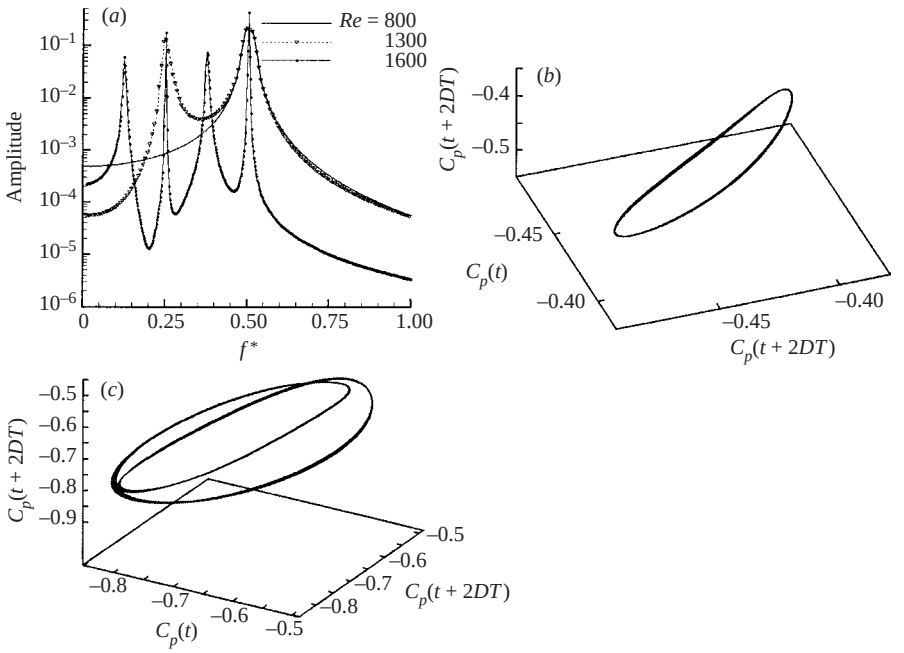

FIGURE 1. (*a*) Pressure coefficient spectra showing the period-doubling mechanism, and the corresponding attractors at (*b*) $Re = 800$ and (*c*) 1300.

number system is determined by the time-delay reconstruction technique (Takens 1980) and is shown in figure 1(*b*, *c*). The three-dimensional projection of the four-dimensional attractor is shown using this method. The first step ($Re = 800$) corresponds to a Poincaré limit cycle due to the appearance of the fundamental as the only dominant frequency. The second step is characterized by the fundamental frequency and its subharmonic ($Re = 1300$). The period-doubling continues, as the Reynolds number increases, as shown in the spectra of figure 1(*a*).

3.2. *The shear-layer instability*

The second mechanism appears beyond $Re = 2000$. The separated shear layer undergoes another important transition mechanism that gives rise to an incommensurate frequency, due to the development of a Kelvin–Helmholtz instability. In the present case, this instability mode is forced by the oscillatory motion of the separation point, which obeys the von Kármán instability. Therefore, the expected dynamics are those of a forced (perturbed) shear layer, according to Ho & Huerre (1984), Freymuth (1966) and Huerre & Monkewitz (1985).

Figure 2 show the progressive undulation of the separated shear layer past the airfoil as well as the clear formation of Kelvin–Helmholtz vortices as the Reynolds number increases from 2000 to 10 000. The shear-layer vortices are shorter than the von Kármán ones and decrease as the Reynolds number increases. A detailed space–time tracking of these vortices allows the evaluation of the shear-layer instability wavelength in the present case. It is found that the wavelength decreases as the Reynolds number increases, according to the law $\lambda_{sl} \propto Re^{-0.44}$ (figure 3*a*). Furthermore the ratio f_{sl}/f_{V-K} is plotted versus Re (figure 3*b*). The variation law obtained is $\propto Re^{0.43}$. This exponent law is very close to the $Re^{0.5}$ that characterizes the development

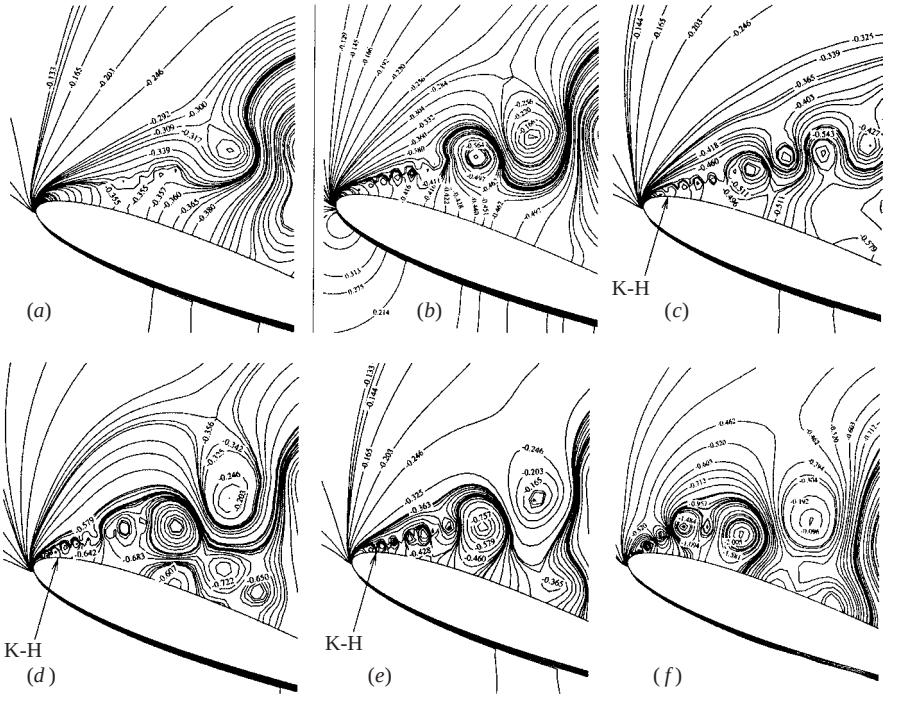

FIGURE 2. Instantaneous iso-pressure contours: spatial view of the shear-layer instability as Reynolds number increases: (*a*) 2000, (*b*) 3000, (*c*) 4000, (*d*) 5000, (*e*) 7000, (*f*) 10 000.

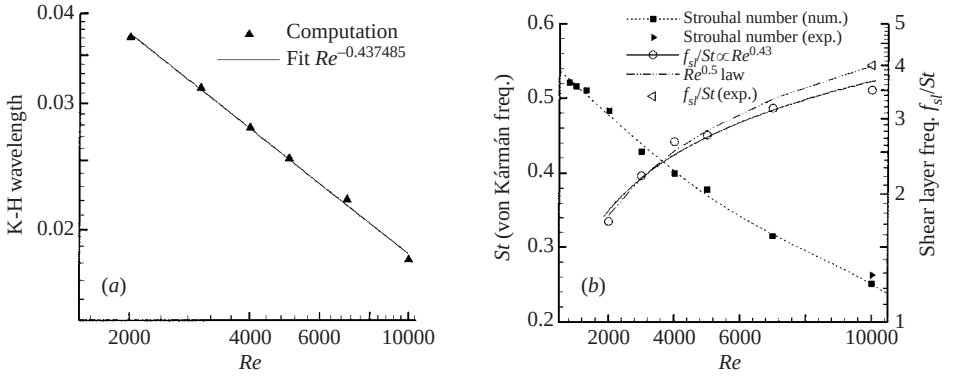

FIGURE 3. Evolution of (*a*) the shear-layer wavelength and (*b*) the Strouhal number and the ratio F_{sl}/S_t, versus the Reynolds number.

of the instability wave prior to separation, as reported by Bloor (1964) for bluff-body wakes.

The shear-layer frequency is an incommensurate mode in comparison to the von Kármán mode. This leads, in association with the period-doubling scenario, to the nonlinear filling of the energy spectrum by a multitude of modes that are combinations of the von Kármán and shear-layer modes, as reported by Braza, Chassaing & Ha-Minh (1990) for bluff-body wakes. The nonlinear interaction of the shear-layer vortices with the von Kármán ones can be followed in figure 2, where the 'tail' of the shear-layer

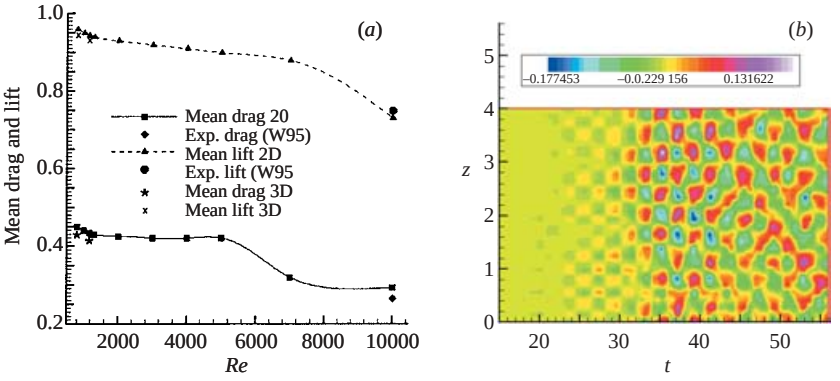

FIGURE 4. Evolution of the global parameters and of the spanwise velocity structure: (*a*) mean drag and lift coefficients versus *Re* (W95 denotes Williamson *et al.* 1995) and (*b*) time–space evolution of the W velocity component along the span, $x/c = 0.7$, $y/c = 0.169$, at $Re = 800$.

vortices region amalgamates with the adjacent von Kármán ones in the formation region.

3.3. *The evolution of the global parameters as the Reynolds number increases*

The global parameters vary with the Reynolds number as a consequence of the above changes, as shown in figures 3(*b*) and 4(*a*). The mean lift coefficient (figure 4*a*) undergoes a smooth decrease as the Reynolds number increases, because the flow is already stalled at 20°, for all the Reynolds numbers examined. Therefore, this decrease corresponds to an equivalent behaviour occurring at fixed *Re* and increased incidence beyond stall. Similarly, the drag coefficient shows a plateau saturation level, attained in the intermediate Reynolds number range, and then decreases as a function of the Reynolds number. The more abrupt decrease of the drag coefficient beyond Reynolds number 5000 is a consequence of the multitude of shear-layer vortices and of the formation of a quasi-stagnation region below the separated shear layer, up to the wall. A comparison of the global parameters is given with the three-dimensional DNS results discussed in the next paragraph. There is a reduction of the three-dimensional drag coefficient, comparing to the two-dimensional one. The same behaviour had been reported by Persillon & Braza (1998) for the cylinder wake. However, the difference between the two- and three-dimensional computations does not exceed about 10% in the present study. This ensures the validity of the two-dimensional approximation in the low *Re*-range with respect to the near-field coherent large-scale structures, that directly influence the drag coefficient.

The Strouhal number evaluated from the lift coefficient follows the shedding motion of the lower trailing-edge vortex, which is delayed by the creation of the above-mentioned fully developed region beyond $Re = 5000$. Therefore, this step is qualitatively similar to the 'drag crisis' appearing in bluff-body wakes at higher Reynolds number, although the wake formation region of a circular cylinder varies significantly in this range. In the crtical regime, a multitude of small-scale vortices are created upstream of the separation, because of the boundary-layer transition occurring there. The Strouhal number versus the Reynolds number (figure 3*b*) also shows a decrease for the same reason. These effects are obtained in the present study by the fully nonlinear approach of the Navier–Stokes system. A comparison of global parameters obtained from the present simulation with a water-channel experiment by Williamson, Govardhan & Prasad (1995) gives very good agreement at Reynolds number 10 000.

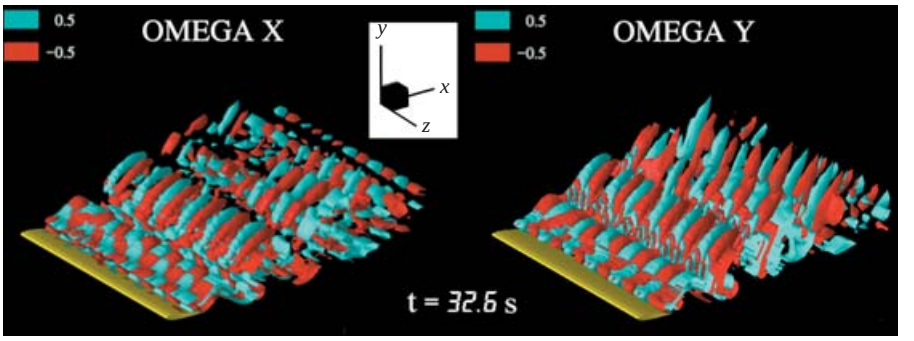

FIGURE 5. Spatial evolution of the longitudinal and vertical vorticity components, $Re = 800$.

Furthermore, the three-dimensional computations in the low *Re*-range found that the Strouhal number is essentially the same as in the two-dimensional case. These facts ensure the validity of the extension of the numerical study from the low to the higher Reynolds number range.

4. The onset of the three-dimensional transition

In this section the development of the three-dimensional transition to turbulence from a nominally two-dimensional flow configuration is examined. The Reynolds number 800 has been selected first, because it corresponds to a very strong and regular development of the von Kármán mode. The initial conditions are either those of a flow at rest triggered by a very weak spanwise W velocity fluctuation imposed as a random fluctuation, or a fully developed two-dimensional vortex shedding pattern perturbed in the same way. The dimensionless r.m.s. values of the spanwise fluctuation are of order $10^{-4}\,U_\infty$. This technique does not predetermine the appearance of any wavelength and the order of magnitude of the fluctuation is very weak and less than the upstream noise existing in any wind tunnel. By performing a very detailed three-dimensional study, it has been found that the flow 'forgets' its initial conditions and both ways of initiating the three-dimensional transition lead to the same final regime: the first step is the development of the two-dimensional von Kármán pattern followed by the appearance of the three-dimensional mechanisms as described below.

4.1. *The history of the three-dimensional transition mechanisms*

Figure 4(*b*) shows the time–space evolution of the W velocity component along the span. After a transient phase, the onset of the three-dimensional transition appears as an organized pattern of the iso-W velocity contours as coherent counter-rotating cells. This step is followed by the amplification of the longitudinal and vertical vorticity components, ω_x and ω_y, that are found to form the same kind of coherent cells, figure 4(*b*). This spanwise-periodic fluctuation plays the role of a factor perturbing the von Kármán rectilinear vortex rows. Consequently, the ω_z vorticity is expected to be modified according to the vorticity conservation equations (Sadeh & Brauer 1980). From elliptic stability theory (Landman & Saffman 1987), the expected spanwise mode of an originally two-dimensional elliptic-shaped vortex (in the present case the von Kármán vortex rows) is a three-dimensional undulated large-scale vortex row with a regular spanwise wavelength. This is shown in figures 5 and 6(*a*). The dynamics of this pattern are similar to those of bluff-body-wake DNS studies (Persillon & Braza 1998), but in the present case the shearing mechanism is totally asymmetric. The shape

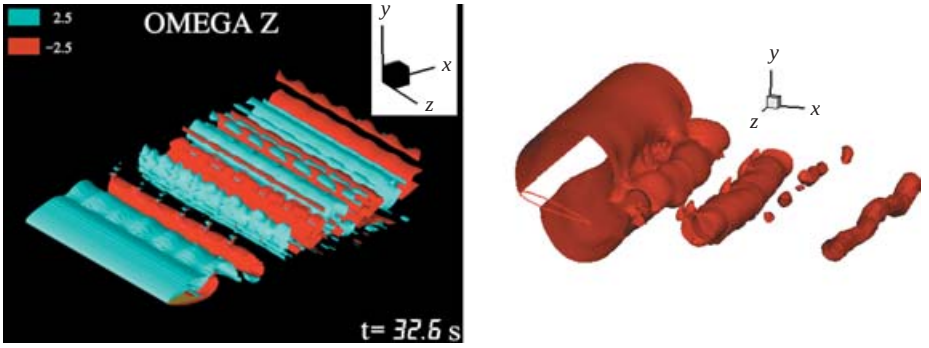

FIGURE 6. Spatial evolution of (*a*) the spanwise vorticity component at $Re = 800$ and (*b*) the pressure coefficient at $Re = 1200$.

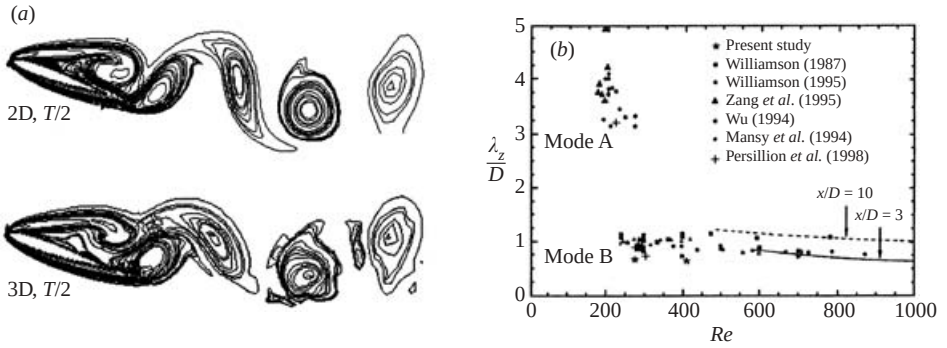

FIGURE 7. (*a*) Comparison of the two- and three-dimensional spanwise-averaged plan at $Re = 800$, (*b*) normalized spanwise wavelength – comparison of cylinder wake (taken from Persillon & Braza 1998) and present study.

of the undulated vortices is much more stretched, with the lifting body configuration. By performing a space-averaging of all the three-dimensional transverse sections at the same instant, it has been proven that the alternating vortex pattern is very similar to the corresponding two-dimensional configuration at the same phase, figure 7(*a*). Therefore, the present three-dimensional route to transition is expected to be affected by the same kind of period-doubling cascade and the shear-layer instability, as discussed in the two-dimensional study. However, the present three-dimensional study is still carried out in a low Reynolds number range where these effects are not yet fully pronounced.

A fast Fourier transform analysis of the spanwise evolution of the secondary instability mode has been used to evaluate the preferential spanwise wavelength developed under the present conditions, $\lambda_z/D = 0.64$. This value is in good agreement with the results for bluff-body wakes: although the fundamentals of the shearing mechanism are different in the present case of lifting-body wakes, an analogy with bluff-body ones can be made by considering an 'equivalent' bluff-body configuration having a characteristic vertical length $c\sin(a)$ in the upstream velocity direction, c being the chord and a the incidence. Therefore, the 'effective' Reynolds number in the wing-body analogue of the bluff body is $Re\, c\sin(20^\circ) = 273$. The expected wavelength for this 'equivalent' bluff-body wake would be of order 0.60–0.70 according to the DNS by Persillon & Braza (1998) and Braza, Persillon & Faghani (2001). The same

kind of three-dimensional dynamics govern the flow at $Re = 1200$, figure 6(*b*), and the corresponding wavelength $\lambda_z/D = 0.62$, at an effective $Re = 410.5$. A qualitative comparison with the cylinder wake is shown in figure 7(*b*). These results are in good qualitative agreement with the three-dimensional wavelength of the bluff-body transition.

The secondary instability development is expected to continue as *Re* increases by providing progressively smaller wavelengths, together with the development of the previously mentioned cascades. Because of the robustness of the two-dimensional alternating pattern even at higher *Re*, it is expected that both routes to transition would persist and be clearly identified as *Re* increases further, by involving in addition nonlinear effects. This study is currently underway within our research group.

5. Conclusion

The present study analyses the successive transition steps in the flow around a high-lift wing configuration, as the Reynolds number increases in the low and moderate range (800–10 000), using the Navier–Stokes approach. A very good agreement is found with a water-channel experiment.

A two-dimensional study has shown that the present flow system is mainly governed by two kinds of organized modes appearing successively as the Reynolds number increases: the von Kármán and the shear layer modes. A period-doubling scenario characterizes the first two-dimensional stages of the von Kármán mode. The shear-layer mode in the flow around an airfoil is characterized. The variation of its dominant streamwise wavelength and of the shear-layer frequency with the Reynolds number is determined.

The successive stages of the three-dimensional transition around a lifting body beyond the first bifurcation are analysed in detail in the low Reynolds number range (800–1200). The history of the three-dimensional mode development and the robustness of the alternating vortex pattern are clearly shown and the spanwise dominant wavelengths are quantified. Next, it would be worthwhile to analyse the period-doubling cascade under the effect of the three-dimensional von Kármán mode at higher Reynolds numbers, as well as the three-dimensional shear-layer transition; this is currently being done in our research group.

The authors are grateful to the French government computer centres CINES, IDRIS and CALMIP for the C.P.U. time attribution. This work was partly supported by the European Commission Research programme UNSI, (Unsteady viscous flows in the context of fluid-structure Interaction), N BRPR-CT97-0583, co-ordinated by EADS.

REFERENCES

Amsden, M. A. & Harlow, F. H. 1970 The SMAC method: a numerical technique for calculating incompressible fluid flows. *Los Alamos Scientific Laboratory Rep.* L.A. 4370.

Bloor, M. 1964 Transition to turbulence in the wake of a circular cylinder. *J. Fluid Mech.* **19**, 290–304.

Bouhadji, A. & Braza, M. 2002 Organised modes and shock-vortex interaction in unsteady transonic flows around an aerofoil. Part I and II. *J. Computers and Fluids* (in press).

Braza, M., Chassaing, P. & Ha-Minh, H. 1986 Numerical study and physical analysis of the pressure and velocity fields in the near wake of a circular cylinder. *J. Fluid Mech.* **165**, 79–130.

Braza, M., Chassaing, P. & Ha-Minh, H. 1990 Prediction of large-scale transition features in the wake of a circular cylinder. *Phys. Fluids* A **2**, 1461–1471.

Braza, M., Persillon, H. & Faghani, D. 2001 Successive stages and the role of natural vortex dislocations in three-dimensional wake transition. *J. Fluid Mech.* **439**, 1–41.

Douglas, J. 1962 Alternating direction methods for three space variables. *Numerische Mathematik* **4**, 41–63.

Feigenbaum, M. J. 1978 Qualitative universality for a class of nonlinear transformations. *J. Statist. Phys.* **19**, 25–52.

Freymuth, P. 1966 On transition in a separated laminar boundary layer. *J. Fluid Mech.* **6**, 683–704.

Ho, C. H. & Huerre, P. 1984 Perturbed free shear layers. *Annu. Rev. Fluid Mech.* **16**, 365–424.

Hoarau, Y. 2002 Analyse physique par simulation numérique et modélisation des écoulements décollés instationnaires autour de surfaces portantes. Thèse de Doctorat de l'INPT.

Hoarau, Y., Rodes, P., Braza, M., Mango, A., Urbach, G., Falandry, P. & Battle, M. 2001 DNS of the 3D transition to turbulence in the incompressible flow around a wing by a parallel implicit navier-stokes solver. In *Proc. Parallel CFD 2000, Trondheim*, pp. 433–440. Elsevier.

Huerre, P. & Monkewitz, P. A. 1985 Absolute and convective instabilities in free shear layers. *J. Fluid Mech.* **159**, 151–168.

Jin, G. & Braza, M. 1993 A non-reflecting outlet boundary condition for incompressible unsteady Navier-Stokes calculations. *J. Comput. Phys.* **107**, 239.

Landman, M. & Saffman, P. 1987 The three-dimensionnal instability of strained vortices in viscous fluid. *Phys. Fluids* **30**, 2339–2342.

McCroskey, W. J. 1982 Unsteady airfoils. *Annu. Rev. Fluid Mech.* **14**, 285–311.

Mehta, U. B. & Lavan, Z. 1975 Starting vortex, separation bubbles and stall: A numerical study of laminar unsteady flow around an airfoil. *J. Fluid Mech.* **67**, 227–256.

Persillon, H. & Braza, M. 1998 Physical analysis of the transition to turbulence in the wake of a circular cylinder by three-dimensional navier-stokes simulation. *J. Fluid Mech.* **365**, 23–88.

Pulliam, T. & Vastano, J. 1993 Transition to chaos in an open unforced 2D flow. *J. Comput. Phys.* **105**.

Sadeh, W. & Brauer, H. J. 1980 A visual investigation of turbulence in stagnation flow about a circular cylinder. *J. Fluid Mech.* **99**, 53–64.

Takens, F. 1980 *Detecting Strange Attractors in Turbulence*. Springer.

Tzabiras, G., Dimas, A. & Loukakis, T. 1986 A numerical method for the calculation of incompressible, steady, separated flows around aerofoils. *Intl J. Numer. Meth. Fluids* **6**, 789–809.

Ventikos, Y. 1995 Numerical investigation of unsteady, cavitating and non-cavitating flows around hydrofoils. PhD Thesis, National Technical University of Athens.

Ventikos, Y., Tzabiras, G. & Braza, M. 1993 The effect of viscous dissipation on the organised structures in the wake past an aerofoil in transition to turbulence. In *Ninth Symp. on Turbulent Shear Flows, Kyoto, Japan, August 16–18* (ed. F. Durst, B. E. Launder, F. W. Schmidt & J. H. Whitelaw). Kyoto University.

Williamson, C., Govardhan, R. & Prasad, A. 1995 Experiments on low Reynolds number NACA0012 aerofoils. *Tech. Rep.* Cornell University.